IEEE Access
Multidisciplinary | Rapid Review | Open Access Journal

Received December 13, 2016, accepted January 3, 2017, date of publication January 10, 2017, date of current version March 6, 2017.

Digital Object Identifier 10.1109/ACCESS.2017.2651043

Channel-Adaptive Space-Collaborative Constellation Design for MIMO VLC With Fast Maximum Likelihood Detection

KE XU, HONG-YI YU, YI-JUN ZHU, (Member, IEEE), AND HENG-BIN CAI
National Digital Switching System Engineering & Technological Research Center, Zhengzhou 450000, China

Corresponding author: Y.-J. Zhu (yijunzhu1976@outlook.com)

This work was supported in part by the China National Science Foundation Council under Grant 61271253 and Grant 61671477 and in part by the Major Scientific and Technological Project of Guangdong Province, China under Grant 2015B010112001. This paper was presented at the IEEE Global Communications Conference 2016, Washington, USA [18].

ABSTRACT Multi-input multi-output (MIMO) holds great potential in the high-speed transmission of visible light communication (VLC). However, as for the current MIMO-VLC techniques, the error performance is improved by wasting spatial resources, which just drops the core advantage within an MIMO structure. Moreover, they cannot change over the channel, which greatly limits their application range. In this paper, a general design criterion of the channel-adaptive space-collaborative constellation (CASCC) is established for MIMO-VLC systems. Specifically, we not only consider the channel into our criterion, but also build relations among the light-emitting diodes to exploit the spatial resources instead of wasting. Under the criterion, a regular CASCC is particularly designed for 2×2 MIMO-VLC in terms of the basic four-point constellation and the high-order constellation. Correspondingly, a fast maximum likelihood (ML) detection algorithm for CASCC is proposed. Simulation results show that our proposed CASCC obtains better error performance and wider application range compared with the conventional MIMO-VLC schemes. Moreover, the fast ML algorithm reduces the computational complexity without any performance loss.

INDEX TERMS Visible light communication, inter-channel interference, space-collaborative, channel-adaptive, fast ML algorithm.

I. INTRODUCTION

In recent years, high-speed transmission of visible light communication (VLC) has attracted substantial attention [1]–[3]. For illumination purpose, multiple lamps are commonly utilized [4]–[6], thus bringing a natural combination of multi-input multi-output (MIMO) and VLC. However, the nonnegative channel and signal in VLC make the majority of techniques in radio frequency (RF) communication inapplicable to MIMO-VLC systems. Among those techniques, repetition coding (RC) emits the same signal from all the light-emitting diodes (LEDs) [7], which can achieve good symbol-error-rate (SER) performance for high correlation MIMO-VLC channels. However, without introducing any channel multiplexing, RC requires large signal constellation to obtain high spectral efficiency. By contrast, spatial modulation (SM) activates merely one of the multiple available lamps to transmit signal at any time instance [8]–[10], which achieves higher spectral efficiency than RC at the expense of the spatial resources. Moreover, spatial multiplexing (SMP) is exploited to transmit independent data from all the LEDs. Although SMP attains better performance, it could not attain the expected gains unless the channel correlation is low enough [11].

However, as for MIMO-VLC systems, there exist two main problems among the above-mentioned techniques.

- Firstly, the error performance is improved by wasting spatial resources to reduce channel correlation, whereas just drop the core advantage within MIMO structure.
- Secondly, they can not change over the channel and a scheme performing good under a channel may perform badly under another channel. Therefore, for geometrical MIMO-VLC, they have a narrow application range.

For VLC, the signals are modulated into the light beams. Typically, the overlapped light beams often cause high channel correlation [12], which is inevitable by merely sacrificing spatial resources. As a promising technique, a space-collaborative constellation (CC) for 2×2 MIMO-VLC was proposed in [15]. By building relations amongst the LEDs,

it obtained better SER performance over RC, SM and SMP. However, since it still could not change over the channel, the error performance changed greatly when the channel moved. Furthermore, [16] designed an optimal constellation with the channel considered, which results showed its better error performance over RC, SM. However, the constellation size in [16] was 2. For high spectral efficiency, it is essential to design the high-order constellation.

Inspired by the above-mentioned factors, in this paper, we establish a general design criterion of the channel-adaptive space-collaborative constellation (CASCC) for MIMO-VLC systems. Specifically, we not only consider the channel into our model, but also build relations among the LEDs to exploit the spatial resources. Then, under the criterion, a regular CASCC is particularly designed for 2×2 MIMO-VLC systems in terms of the basic 4-point constellation and the high-order constellation. For simplifying the design, we transform the model from 8 variables to 2 variables by developing some mathematical properties. Correspondingly, a fast maximum likelihood (ML) detection algorithm for CASCC is proposed. Finally, the performance of the CASCC and fast ML algorithm are discussed by simulation analysis in detail.

Note that we list the key notations throughout the paper in Table I for conciseness.

TABLE 1. Key notations used in this paper.

Notations	Explanation
$\mathcal{S}$, $\mathcal{R}$	Constellation at transmitter, receiver
$\mathcal{S}_B$, $\mathcal{R}_B$	Basic constellation at transmitter, receiver
Q_x, Q_y	Quadrilateral for constellation $\mathcal{S}_B$, $\mathcal{R}_B$
$\mathcal{S}_E$	Extension constellation at the transmitter
P_T	Total electrical power
$\mathbf{\Omega}$	Feasible constellations region to Model 1
l_f	Side length of Q_y
α_f	Angle between two adjacent sides of Q_y
$d_{\mathcal{R}m}$	Minimum ED at the receiver
L	Number of constellation points
β_i, x, y	Introduced variables
N_e	Number of 2-norms $\|\cdot\|$
N_a	Number of additions/subtractions
N_m	Number of multiplications
B	Spectral efficiency

II. SYSTEM MODEL AND CONSTELLATION CRITERION

A. SYSTEM MODEL

In this paper, let us consider a MIMO-VLC system with N_t LEDs as transmitters and N_r photo-detectors (PDs) as receivers. As shown in Fig. 1, the input information is modulated to form an input data vector $\mathbf{x} = \left(x_1, x_2, \cdots, x_{N_t}\right)^T \in \mathcal{S}^{N_t}$, where $\mathcal{S}$ is a given modulation constellation at the transmitter. Then the received signal vector $\mathbf{y}$ is given by

$$\mathbf{y} = \mathbf{H}\mathbf{x} + \mathbf{n}, \tag{1}$$

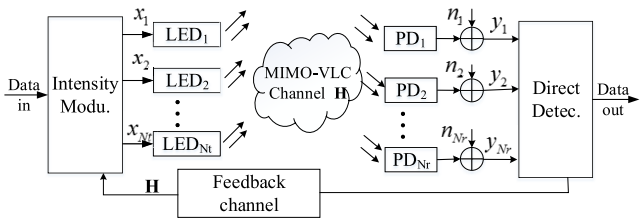

FIGURE 1. The MIMO-VLC system model with H known at the transmitter.

where $\mathbf{n}$ denotes $N_r \times 1$ real valued additive white Gaussian noise (AWGN) with zero mean and covariance matrix $\sigma^2\mathbf{I}_{N_r}$ [1], [3]. $\mathbf{H}$ is a $N_r \times N_t$ channel matrix and known at the transmitters.[1] Typically, we consider an indoor scenario with the line of sight (LOS) characteristic [11], and h_{ij} is non-negative and real, which is determined by [1], [3]

$$h_{ij} = \begin{cases} \dfrac{A_r\,(m+1)}{2\pi D_{ij}^2}\cos^m(\phi)\cos(\psi), & 0 \le \psi \le \Psi_c \\ 0, & \psi > \Psi_c, \end{cases} \tag{2}$$

where ϕ is the angle of emergence with respect to the transmitter axis and ψ is the angle of incidence with respect to the receiver axis. The Lambertąs mode order m is related to the half power semiangle $\Phi_{\frac{1}{2}}$ via $m = \frac{-\ln 2}{\ln(\cos \Phi_{\frac{1}{2}})}$. A_r denotes the effective area of the detector and Ψ_c is the field-of-view (FOV) semiangle of the detector. D_{ij} depicts the distance between the jth LED and ith PD.

In VLC, there are three power measurements: the electrical power, the optical power and the peak power. Due to that they can be mutually converted [18], let us consider the common average electrical power, $\bar{P}_e = \frac{\mathbb{E}[\|\mathbf{x}\|_2^2]}{T_s}$, $\mathbf{x} \in \mathcal{S}$, where $\mathbb{E}[\cdot]$ is an expectation operator and T_s is the symbol period [18]. If $|\mathcal{S}| = L$, the total electrical power at the transmitter is $P_T = |\mathcal{S}|\bar{P}_e = \sum_{\mathbf{s}\in\mathcal{S}} \|\mathbf{s}\|_2^2$.

B. CONSTELLATION CRITERION

Our design criterion for MIMO-VLC systems is mainly based on two major features as follows:

- *Channel Adaptive:*Although MIMO-VLC channel is time-invariant, it changes with the geometrical locations of transmitters and receivers. To widen the application range, the channel-adaptive constellation should be designed. Our objective function is based on the Euclidean distance (ED) of constellation at the receiver, $\|\mathbf{H}\mathbf{s} - \mathbf{H}\hat{\mathbf{s}}\|_2$, instead of that at the transmitter, $\|\mathbf{s} - \hat{\mathbf{s}}\|_2$.
- *Space Collaborative:* Initially, incorporating MIMO and VLC is for high data rate by using the spatial resources. To exploit rather than sacrificing the spatial resouces, we build relations within the LEDs and thus design a space-collaborative constellation, of which each dimension maps the corresponding LED.

[1]Note that the availability of CSIT is not a strong assumption in OWC, whose coherence time is typically much larger than the symbol duration [19]. Thus, estimation and feedback of the channel state can be achieved in negligible time without considerably affecting performance.

Then, we conclude the criterion of CASCC as follows.

Criterion 1: For MIMO-VLC systems, our constellation structure is

$$\mathcal{R} = \mathbf{H}\mathcal{S}, \tag{3}$$

where $\mathbf{H} \succeq 0$, $\mathcal{S} = [\mathbf{s}_1, \mathbf{s}_2, ..., \mathbf{s}_L]$, $\mathbf{s}_i = \left(s_{i1}, s_{i2}, \cdots, s_{iN_t}\right)^T$ is the constellation at the transmitter, $\mathcal{R} = [\mathbf{r}_1, \mathbf{r}_2, ..., \mathbf{r}_L]$, $\mathbf{r}_i = \left(r_{i1}, r_{i2}, \cdots, r_{iN_r}\right)^T$ is the corresponding constellation at the receiver. $|\mathcal{S}| = L$ represents the constellation size and $p = \log_2 L$ denotes its constellation order. $\mathbf{s}_i$ depicts the ith spatial constellation point and $s(i, j)$ expresents the jth LED of the ith point, $i \in \{1, ..., L\}, j \in \{1, ..., N_t\}$.

Then, relying on the constellation structure, our optimization criterion is formulated as finding the optimal $\mathcal{S}$ at the transmitter that maximizes $d_{\mathcal{R}m}$ of $\mathcal{R}$ at the receiver, subject to the fixed total electrical power P_T of $\mathcal{S}$, i.e.,

$$\begin{aligned} &\arg\max_{\mathcal{S}} d_{\mathcal{R}m} = \min_{s\neq\hat{s},s,\hat{s}\in\mathcal{S}} \|\mathbf{Hs} - \mathbf{H}\hat{\mathbf{s}}\|_2 \\ &s.t. \begin{cases} \sum_{\mathbf{s}\in\mathcal{S}} \|\mathbf{s}\|_2^2 = P_T \\ \mathcal{S} \succeq 0. \end{cases} \end{aligned} \tag{4}$$

III. OPTIMIZATION MODEL OF CONSTELLATION DESIGN

In this section, our criterion is exemplified for 2×2 MIMO-VLC, i.e., $N_t = N_r = 2$. We firstly formulate the optimization model, then develop some mathematical preliminaries and finally get the simplified optimization model.

A. ORIGINAL OPTIMIZATION MODEL

Since four adjacent constellation points are often viewed as the basic unit of constellation, we will design CASCC in two aspects: firstly to design the basic 4-point constellation $\mathcal{S}_B$, and then to extend $\mathcal{S}_B$ to the high-order constellation $\mathcal{S}_E$.

Note that the quadrilaterals for $\mathcal{S}_B$, $\mathcal{R}_B$ are denoted as Q_x, Q_y. Notation Ω represents the feasible set for $\mathcal{S}_B$ meeting the constraints in (4). Two statements regarding $\mathcal{S}_B$ are made as

- *Constellation Mapping.* Let $\Delta\mathbf{R}_{2\times4} = \mathbf{H}\Delta\mathbf{S}_{2\times4}$, where $\Delta\mathbf{R}_{2\times4} = [\Delta\mathbf{r}_a, \Delta\mathbf{r}_b, \Delta\mathbf{r}_c, \Delta\mathbf{r}_d] = [\mathbf{r}_2 - \mathbf{r}_1, \mathbf{r}_3 - \mathbf{r}_2, \mathbf{r}_4 - \mathbf{r}_3, \mathbf{r}_1 - \mathbf{r}_4]$, $\Delta\mathbf{S}_{2\times4} = [\Delta\mathbf{s}_a, \Delta\mathbf{s}_b, \Delta\mathbf{s}_c, \Delta\mathbf{s}_d] = [\mathbf{s}_2 - \mathbf{s}_1, \mathbf{s}_3 - \mathbf{s}_2, \mathbf{s}_4 - \mathbf{s}_3, \mathbf{s}_1 - \mathbf{s}_4]$. So, there is a one-to-one mapping between $\Delta\mathbf{R}_{2\times4}$ and $\Delta\mathbf{S}_{2\times4}$ via $\mathbf{H}$, so is $\mathcal{S}$ and $\mathcal{R}$ in (3). Note that the subscripts $\{1, 2, 3, 4\}$ above are for $\mathcal{S}_B$, $\mathcal{R}_B$, while $\{a, b, c, d\}$ are for $\Delta\mathbf{S}$, $\Delta\mathbf{R}$.
- *Partition of Feasible Set* Ω. Due to that Q_y includes two cases: a diamond that $\|\Delta\mathbf{r}_a\|_2 = \|\Delta\mathbf{r}_b\|_2 = \|\Delta\mathbf{r}_c\|_2 = \|\Delta\mathbf{r}_d\|_2$ or the opposite, set Ω can be partitioned into $\mathcal{N}_1$ and $\mathcal{N}_2$, i.e.,

$$\Omega = \mathcal{N}_1 \cup \mathcal{N}_2, \mathcal{N}_1 \cap \mathcal{N}_2 = \varnothing. \tag{5}$$

  Q_y mapped by each element in $\mathcal{N}_1$ is a diamond, while Q_y mapped by each element in $\mathcal{N}_2$ is the opposite. To get a regular constellation easy to be extended or detected, we focus on the region of $\mathcal{N}_1$.

Then, the optimization model could be rewritten as:

Model 1: For 2×2 MIMO-VLC $\mathbf{H}(\succeq 0)$, we formulate our optimization model for the basic constellation $\mathcal{S}_B = \left[\mathbf{s}_1\ \mathbf{s}_2\ \mathbf{s}_3\ \mathbf{s}_4\right]$, $\mathbf{s}_i = [s_{i1}, s_{i2}]^T$ as:

$$\begin{aligned} &\arg\max_{\mathcal{S}_B} \quad d_{\mathcal{R}m} = \min_{s\neq\hat{s},s,\hat{s}\in\mathcal{S}} \|\mathbf{Hs} - \mathbf{H}\hat{\mathbf{s}}\|_2 \\ &s.t. \begin{cases} \|\mathbf{s}_1\|_2^2 + \|\mathbf{s}_2\|_2^2 + \|\mathbf{s}_3\|_2^2 + \|\mathbf{s}_4\|_2^2 = P_T \\ \mathcal{S}_B \in \mathcal{N}_1. \end{cases} \end{aligned} \tag{6}$$

B. MATHEMATICAL PRELIMINARIES

In this subsection, we will make some mathematical preliminaries for transforming Model 1. Note that all the proofs of the following Lemmas are given in Appendices.

Lemma 1: In $\mathcal{N}_1$, the quadrilateral Q_x of the optimal constellation $\mathcal{S}_B$ is a parallelogram. Moreover, the slopes of all sides are nonnegative. ■

Lemma 2: In $\mathcal{N}_1$, the origin is included in the optimal constellation $\mathcal{S}_B$, i.e. $(0, 0)^T \in \mathcal{S}_B$. ■

The above Lemmas 1 and 2 are about the special structure of constellation $\mathcal{S}_B$. Next, by analyzing the channel, we transform the constraints and the objective function of Model 1, respectively. Note that the diamond Q_y ($\in \mathcal{N}_1$) can be expressed by two parameters of the side length l_f and the angle α_f between two adjacent sides as shown in Fig. 2(b).

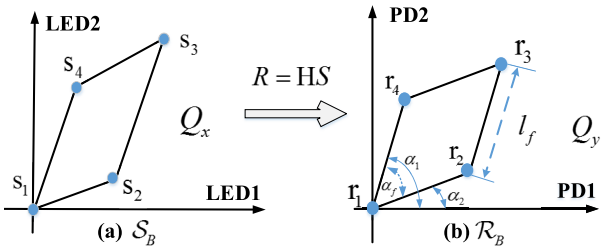

FIGURE 2. The constellation maps for $\mathcal{S}_B$ at the transmitter (a) and $\mathcal{R}_B$ at the receiver (b) via 2 × 2 MIMO-VLC channel H.

1) CHANNEL ANALYSIS

Using Perron-Frobenius Theorem [20], we have $\mathbf{H}^T\mathbf{H} = \mathbf{V}\Lambda\mathbf{V}^T$, where $\mathbf{V} = \begin{bmatrix} \cos\varphi & -\sin\varphi \\ \sin\varphi & \cos\varphi \end{bmatrix}$ for $\varphi \in \left[0, \frac{\pi}{2}\right]$ and $\Lambda = \text{diag}\left\{\lambda_1^2, \lambda_2^2\right\}$ with $\lambda_1 \geq \lambda_2 \geq 0$ being the singular values of $\mathbf{H}$.

- *As for* λ_1, λ_2. There exist two situations of $\lambda_1 \geq \lambda_2 > 0$, $\lambda_1 > \lambda_2 = 0$.
- *As for* φ. There exist three cases about φ. Case I: $0 < \varphi < \frac{\pi}{2}$, Case II: $\varphi = 0$ and Case III: $\varphi = \frac{\pi}{2}$.

2) TRANSFORMATIONS OF CONSTRAINTS

We analyze the constraints from $\lambda_1 \geq \lambda_2 > 0$, $\lambda_1 > \lambda_2 = 0$, as follows.

Lemma 3: For the channel meeting $\lambda_1 \geq \lambda_2 > 0$, we transform the constraints of 8 variables in (6) to the expressions of two parameters β_a, β_d, under different cases of φ.

For Case I, two parameters β_a, β_d are subject to $-\frac{\lambda_2 \tan\varphi}{\lambda_1} \leq \tan\beta_a \leq \frac{\lambda_2 \cot\varphi}{\lambda_1}$, $-\frac{\lambda_2 \tan\varphi}{\lambda_1} \leq \tan\beta_d \leq \frac{\lambda_2 \cot\varphi}{\lambda_1}$

and $\cos\beta_a > 0, \cos\beta_d < 0$. As for α_f, if $\alpha_f \neq 0$ and $\alpha_2 = 0$, then $\tan\alpha_f = \frac{\lambda_2\cos\varphi - \lambda_1\sin\varphi\tan\beta_d}{\lambda_2\sin\varphi + \lambda_1\cos\varphi\tan\beta_d}$. If $\alpha_f \neq 0$ and $\alpha_1 = \frac{\pi}{2}$, then $\alpha_f = \frac{\pi}{2} - \arctan\frac{\lambda_2\cos\varphi - \lambda_1\sin\varphi\tan\beta_a}{\lambda_2\sin\varphi + \lambda_1\cos\varphi\tan\beta_a}$. If $\alpha_f \neq 0, \alpha_1 \neq \frac{\pi}{2}$ and $\alpha_2 \neq 0$, then we have $\tan\alpha_f = \frac{\xi\sin(\beta_a - \beta_d)}{\cos\beta_a\cos\beta_d + \sin\beta_a\sin\beta_d}$, where $\xi = \frac{(h_{12}h_{21} - h_{22}h_{11})}{\lambda_1\lambda_2}$. Obviously, $\xi = 1$ or -1.

For Case II, the parameters β_a, β_d are subject to $\beta_a \in [0, \frac{\pi}{2}]$ and $\beta_d \in [\pi, \frac{3\pi}{2}]$. As for α_f, if $\alpha_f \neq 0$ and $\alpha_2 = 0$, then $\tan\alpha_f = \frac{\lambda_2\cos\beta_d}{\lambda_1\sin\beta_d}$. If $\alpha_f \neq 0$ and $\alpha_1 = \frac{\pi}{2}$, then $\alpha_f = \frac{\pi}{2} - \arctan\frac{\lambda_2\cos\beta_a}{\lambda_1\sin\beta_a}$. If $\alpha_f \neq 0, \alpha_1 \neq \frac{\pi}{2}$ and $\alpha_2 \neq 0$, then α_f matches the same expression as Case I.

For Case III, the parameters β_a, β_d are subject to $\beta_a \in [\frac{3\pi}{2}, 2\pi]$, $\beta_d \in [\frac{\pi}{2}, \pi]$. As for α_f, if $\alpha_f \neq 0$ and $\alpha_2 = 0$, then $\tan\alpha_f = \frac{-\lambda_1\sin\beta_d}{\lambda_2\cos\beta_d}$. If $\alpha_f \neq 0$ and $\alpha_1 = \frac{\pi}{2}$, then $\alpha_f = \frac{\pi}{2} + \arctan\frac{\lambda_1\sin\beta_a}{\lambda_2\cos\beta_a}$. If $\alpha_f \neq 0, \alpha_1 \neq \frac{\pi}{2}$ and $\alpha_2 \neq 0$, then α_f matches the same expression as Case I. ■

Lemma 4: For the channel of $\lambda_1 > \lambda_2 = 0$, there exist no feasible constellations to Model 1, regardless of the value φ in $[0, \frac{\pi}{2}]$. ■

3) TRANSFORMATIONS OF OBJECTIVE FUNCTIONS

Because the minimum ED $d_{\mathcal{R}m}$ of Q_y may be at the sides or diagonals, we divide Set $\mathcal{N}_1$ into $\mathcal{M}_1$ for the former case and $\mathcal{M}_2$ for the latter case, i.e.,

$$\mathcal{N}_1 = \mathcal{M}_1 \cup \mathcal{M}_2, \quad \mathcal{M}_1 \cap \mathcal{M}_2 = \varnothing. \tag{7}$$

Apparently, $\tan\alpha_f \geq \sqrt{3}$ for $\mathcal{M}_1$ and $0 \leq \tan\alpha_f < \sqrt{3}$ for $\mathcal{M}_2$. Correspondingly, Model 1 can be decomposed into two submodels. We denote the minimum ED of Q_y for $\mathcal{M}_1$ as $d_{\mathcal{R}m1}$ and for $\mathcal{M}_2$ as $d_{\mathcal{R}m2}$. Note that the manners under three cases of φ are similar, so we merely take Case I as example in the follwing Lemma 5.

Lemma 5: For Case I, with fixed total power P_T, we have

$$l_f^2 = \frac{P_T}{2T}, \tag{8}$$

where $T = \frac{\cos^2\beta_a + \cos^2\beta_d - \cos\beta_a\cos\beta_d}{\lambda_1^2} + \frac{\sin^2\beta_a\sin^2\beta_d - \sin\beta_a\sin\beta_d}{\lambda_2^2}$.

For the submodel in $\mathcal{M}_1$, $d_{\mathcal{R}m1} = l_f$. The relation of $d_{\mathcal{R}m1}$ with β_a, β_d is $T = \frac{P_T}{(2d_{\mathcal{R}m1}^2)}$, and the corresponding objective function is simplified as minimizing T.

For the submodel in $\mathcal{M}_2$, the relation of $d_{\mathcal{R}m2}$ with β_a, β_d is $d_{\mathcal{R}m2}^2 = \frac{P_T(1-\cos\alpha_f)}{T}$, and the objective function is simplified as maximizing $d_{\mathcal{R}m2}$. ■

C. SIMPLIFIED OPTIMIZATION MODEL

Based on the above lemmas, Model 1 with 8 variables in $\mathcal{S}_B$ can be transformed to two submodels with 2 introduced variables. Since the same methods are applied to three cases of φ, we take Case I as example here.

For conciseness, we convert the parameters β_a, β_d above to x, y by the relations of

$$x \triangleq \tan\beta_a, \quad y \triangleq \tan\beta_d. \tag{9}$$

Owing to $\cos\beta_a > 0, \cos\beta_d < 0$ in Lemma 3, we get $\cos\beta_a = \frac{1}{\sqrt{1+x^2}}, \cos\beta_d = \frac{-1}{\sqrt{1+y^2}}$, $\sin\beta_a = \frac{x}{\sqrt{1+x^2}}, \sin\beta_d = \frac{-y}{\sqrt{1+y^2}}$. Furthermore, $\tan\alpha_f$ and T in Lemma 3 are transformed to $\tan\alpha_f = \frac{\xi(x-y)}{1+xy}$,

$$T = \frac{1}{\lambda_1^2}\left(\frac{1}{1+x^2} + \frac{1}{1+y^2} + \frac{1}{\sqrt{(1+x^2)(1+y^2)}}\right) + \frac{1}{\lambda_2^2}\left(\frac{x^2}{1+x^2} + \frac{y^2}{1+y^2} + \frac{xy}{\sqrt{(1+x^2)(1+y^2)}}\right).$$

Then, Model 1 is finally simplified as the following two submodels.

Submodel 1: (For $\mathcal{M}_1$) Find the solution $x_{opt1}, y_{opt1}, d_{\mathcal{R}m1}$ to the optimization submodel:

$$\arg\min_{x,y} T \quad s.t. \begin{cases} -\frac{\lambda_2\tan\varphi}{\lambda_1} \leq x \leq \frac{\lambda_2\cot\varphi}{\lambda_1} \\ -\frac{\lambda_2\tan\varphi}{\lambda_1} \leq y \leq \frac{\lambda_2\cot\varphi}{\lambda_1} \\ \tan\alpha_f = \frac{\xi(x-y)}{1+xy} \geq \sqrt{3}. \end{cases} \tag{10}$$

Submodel 2: (For $\mathcal{M}_2$) Find the solution $x_{opt2}, y_{opt2}, d_{\mathcal{R}m2}$ to the optimization submodel:

$$\arg\max_{x,y} \quad d_{\mathcal{R}m2}^2 = \frac{P_T(1-\cos\alpha_f)}{T} \quad s.t. \begin{cases} -\frac{\lambda_2\tan\varphi}{\lambda_1} \leq x \leq \frac{\lambda_2\cot\varphi}{\lambda_1} \\ -\frac{\lambda_2\tan\varphi}{\lambda_1} \leq y \leq \frac{\lambda_2\cot\varphi}{\lambda_1} \\ 0 \leq \tan\alpha_f = \frac{\xi(x-y)}{1+xy} < \sqrt{3}. \end{cases} \tag{11}$$

Algorithm 1 Design of the Basic Constellation $\mathcal{S}_B$

1) Through the eigenvalue decomposition $\mathbf{H}^T\mathbf{H} = \mathbf{V}\Lambda\mathbf{V}^T$, get λ_1, λ_2, φ and ξ of $\mathbf{H}$.
2) Get the specific Submodel 1, and find the corresponding optimal solution x_{opt1}, y_{opt1}, $d_{\mathcal{R}m1}$.
3) Get the specific Submodel 2, and find the corresponding optimal solution x_{opt2}, y_{opt2}, $d_{\mathcal{R}m2}$.
4) choose the larger one of $d_{\mathcal{R}m1}$, $d_{\mathcal{R}m2}$ and get $\Delta\mathbf{S}_{opt}$ from the relations of x, y with β_a, β_d in (9).
5) From $\Delta\mathbf{S}_{opt}$, we can get the optimal basic constellation $\mathcal{S}_B = [\mathbf{s}_1\ \mathbf{s}_2\ \mathbf{s}_3\ \mathbf{s}_4]$, where

$$\mathbf{s}_1 = [0\ 0]^T, \ \mathbf{s}_2 = \Delta\mathbf{s}_{aopt}, \quad \mathbf{s}_4 = -\Delta\mathbf{s}_{dopt}, \ \mathbf{s}_3 = \Delta\mathbf{s}_{aopt} - \Delta\mathbf{s}_{dopt}. \tag{12}$$

IV. CONSTELLATION DESIGN AND FAST DETECTION ALGORITHM

A. CONSTELLATION DESIGN

In this subsection, we give our designs of CASCC in terms of the basic constellation $\mathcal{S}_B$ and the high-order constellation $\mathcal{S}_E$ as follows:

Algorithm 2 Design of the Extension Constellation $\mathcal{S}_E$

The extension constellation $\mathcal{S}_E$, $|\mathcal{S}_E| = 2^p$, includes two cases: even p and odd p.

1) Even p. For $m \in [1, 2^p]$, we have $g = \sqrt{2^p}$, $r = \left\lceil \frac{m}{g} \right\rceil$ and $v = m - (r-1)\,g$. Then

$$\begin{cases} S_E\,(1, m) = (v-1)\,s_{21} + (r-1)\,s_{41} \\ S_E\,(2, m) = (v-1)\,s_{22} + (r-1)\,s_{42}. \end{cases} \tag{13}$$

2) Odd p. Extend $\mathcal{S}_B$ to $\mathcal{S}_E$, $(m \in [1, 2^p])$, as
i) Find w that meets $(w-1)^2 \le 2^p \le w^2$.
ii) For $m \in [1, w^2]$, $r = \left\lceil \frac{m}{w} \right\rceil$, $v = m - (r-1)w$, and calculate $\mathcal{S}_E(:, m)$ as (13).
iii) Compute the ED of $\mathcal{S}_E(:, m)$ to the origin, denoted as e_m. Sort e_m, $m \in [1, w^2]$ and remove $w^2 - 2^p$ points that have the larger e_m from w^2 points. Then, the remaining 2^p points form $\mathcal{S}_E$.

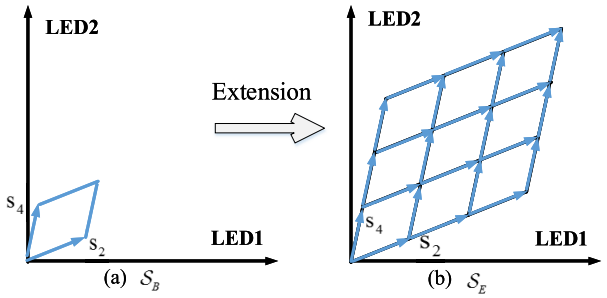

FIGURE 3. At the transmitter, the constellation extension from the basic constellation $\mathcal{S}_B$ (a) to the extension constellaion $\mathcal{S}_E$ (b).

1) DESIGN OF $\mathcal{S}_B$

The basic constellation $\mathcal{S}_B$ can be designed as:

2) DESIGN OF $\mathcal{S}_E$

Inspired by the relation of 4QAM with MQAM, we design $\mathcal{S}_E$ based on two vectors $\mathbf{s}_2 = [s_{21}, s_{22}]^T$ and $\mathbf{s}_4 = [s_{41}, s_{42}]^T$ of $\mathcal{S}_B$. Fig. 3 shows our sketch for the constellation extension. Then, we can summarize the design of the extension constellation in Algorithm 2[2] at next page.

B. FAST MAXIMUM LIKELIHOOD DETECTION

According to the ML principle, each received signal vector $\mathbf{y}_i$ can be detected by

$$\hat{\mathbf{y}}_i = \arg\min_{\mathbf{r}\in\mathcal{R}} \|\mathbf{y}_i - \mathbf{r}\|^2. \tag{14}$$

The search region in (14) is the whole $\mathcal{R}$. For transmission, the constellation size $|\mathcal{R}|$ for the spectral efficiency B should be 2^B. Then, the number of 2-norm $\|\cdot\|^2$ in (14) are exponential to the spectral efficiency, i.e., 2^B, which causes high computational complexity for detection.

[2]Note that we mainly consider the energy-efficiency into the extension here, while more factors can be considered for the future work.

Next, we propose a fast ML detection algorithm, which differs from (14) in the search region. We reduce the search region by analyzing the following features of $\mathcal{R}$ in (3).

- *Another type expression of* $\mathcal{R}$. It is evident that $\mathcal{R}$ is known at the receiver. As shown in Fig. 4(a), $\mathcal{R}$ is regular and can be expressed by two basic vector $\mathbf{b}_{r1} = [b_{r11}, b_{r12}]^T = \mathbf{H}\mathbf{s}_2$, $\mathbf{b}_{r2} = [b_{r21}, b_{r22}]^T = \mathbf{H}\mathbf{s}_4$. So, $\mathbf{b}_{r1}, \mathbf{b}_{r2}$ are also known at the receiver.
- *The reduced search region.* According to (3), if there exist no noises, each transmitted signal vector $\mathbf{x}_i$ from $\mathcal{S}$ should map the corresponding vector $\mathbf{z}_i$ of $\mathcal{R}$ via $\mathbf{H}$. Then, for the practical channel with noises, the received signal vector $\mathbf{y}_i$ are very likely to scatter the $\mathbf{z}_i$-adjacent region $\mathcal{G}_i$ in $\mathcal{R}$. Here, $\mathbf{z}_i \in \mathcal{G}_i$. Particularly, it is easy to get $\mathcal{G}_i$ from the regular and known $\mathcal{R}$.

In Fig. 4, (a) depicts $\mathbf{b}_{r1}, \mathbf{b}_{r2}$, while (b)(c)(d) give three basic cases of $\mathcal{G}_i$. When $\mathbf{z}_i$ is at the corner, $|\mathcal{G}_i|$ includes 4 elements. When $\hat{\mathbf{z}}_i$ lies in the edge, $|\mathcal{G}_i|$ has 6 elements. When $\hat{\mathbf{z}}_i$ is at the inner , $|\mathcal{G}_i|$ includes 9 elements. The other cases are just a simple conversion of the basic cases. From two features above, we give the fast detection in Algorithm 3.

Algorithm 3 Fast ML Detection Algorithm

1) For ith receiver vector $\mathbf{y}_i$, make an initial detection as

$$\hat{\mathbf{z}}_i = \left(round(\frac{\mathbf{y}_i(1)}{br_{11}}), round(\frac{\mathbf{y}_i(2)}{br_{22}}) \right)^T. \tag{15}$$

As the function $round(x)$, if $x \ge 0$, $round(x)$ is the integral most close to x. If $x < 0$, $round(x) = 0$.

2) From $\mathcal{R}$, it is easy to get the search region $\mathcal{G}_i$ based on the locations of $\hat{\mathbf{z}}_i$. Then compare $\mathbf{y}_i$ with the elements in $\mathcal{G}_i$, and the detected signal

$$\hat{\mathbf{y}}_i = \arg\min_{\mathbf{r}\in\mathcal{G}_i} \|\mathbf{y}_i - \mathbf{r}\|^2. \tag{16}$$

C. SOME REMARKS

We make some remarks about our constellation and fast algorithm.

1) COMPUTATIONAL COMPLEXITY OF DETECTION ALGORITHM

Let us denote the number of 2-norm $\|\cdot\|$, additions/subtractions, multiplications as N_e, N_a and N_m, respectively. For the spectral efficiency B, the number of 2-norms for $\mathbf{y}_i$ in (14) is 2^B. By contrast, the number of 2-norms for $\mathbf{y}_i$ in (16) is $|\mathcal{G}_i|$ $(\le 2^B)$. Then, for conventional ML detection in (14),

$$\begin{aligned} N_e &= 2^B, \quad N_m = N_e N_t, \\ N_a &= N_e(2N_t - 1) + N_e \log N_e. \end{aligned} \tag{17}$$

For Algorithm 3,

$$\begin{aligned} N_e &= \frac{\sum_{i=1}^{2^B} |\mathcal{G}_i|}{2^B}, \quad N_m = N_e N_t + 2, \\ N_a &= N_e(2N_t - 1) + N_e \log N_e. \end{aligned} \tag{18}$$

Taking Fig. 4 for example, $B = 4$ and $N_t = 2$. In Fig. 4(a), the number existing (b) is 4, the number existing (c) is 8, and the number existing (d) is 4. Finally, N_e for Algorithm 3 is $N_e = \frac{4*4+8*6+4*9}{16} = 6.25$, whereas $N_e = 16$ in (14). Moreover, the larger spectral efficiency, the more advantage of our fast detection algorithm. More analysis about the complexity and error performance are given in Section V.

2) UTILIZATION OF SPATIAL RESOURCES

Different from the existing techniques, CASCC exploits the spatial resources by building relations amongst LEDs. Fig. 2 shows the sketch map of CASCC in (3). Fig. 5(a) and (b) plots the maps of SM and RC in our space-collaborative constellation coordinate. SM is build on two LED axes and RC on the diagonal, whereas our CASCC extends the feasible region to the first octant.

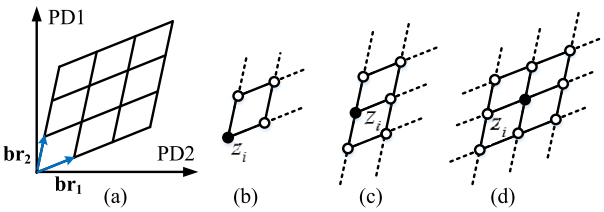

FIGURE 4. The maps for $\mathcal{R}$ (a) and three basic cases of search regions (b) at the corner, (c) at the edge, (d) at the inner.

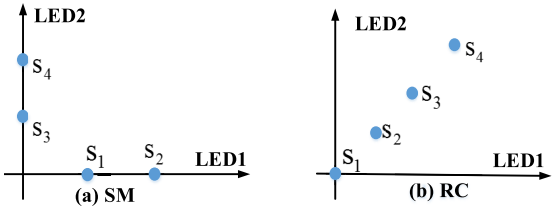

FIGURE 5. The maps of SM (a) and RC (b) in our constellation coordinate.

3) OPTIMALITY ANALYSIS OF CASCC

Within our analysis, we explore the region of $\mathcal{N}_1$ to develop a regular constellation, thus $\mathcal{S}_B$ is optimal within $\mathcal{N}_1$. As the case of $\lambda_1 > \lambda_2 = 0$ is not included in $\mathcal{N}_1$, our CASCC is not applicable to the channel scenario of $\lambda_1 > \lambda_2 = 0$, as Lemma 4. In contrast to CC in [16], since it does not consider the channel $\mathbf{H}$, CC is not optimal at the receiver and thus obtains less gains than our CASCC. Furthermore, due to that the EDs among adjacent constellation points of SM are not equal, the SER is often approximated by union bound methods [7], making it difficult to make a rigorous comparison of CASCC and SM. As an exploration, we provide Theorem 1, the proof of which is postponed into Appendix *E*. Note that we do not compare CASCC with RC here, with the performance between RC and SM having been analyzed in [7].

Theorem 1: For 2×2 MIMO-VLC systems, our CASCC in Designs 1 and 2 achieves gains over SM for $\mathbf{H}$ subject to

$$\frac{|det(\mathbf{H})|}{h_{21}h_{11} + h_{12}h_{22}} \geq \sqrt{3}, \quad \mathbf{H} \triangleq \begin{bmatrix} h_{11} & h_{21} \\ h_{12} & h_{22} \end{bmatrix}, \tag{19}$$

which is sufficient but unnecessary. Specifically, $0 \leq \alpha \leq 2 - \sqrt{3}$ for the symmetric channel $\mathbf{H} \triangleq \begin{bmatrix} 1 & \alpha \\ \alpha & 1 \end{bmatrix}$.

V. COMPUTER SIMULATIONS

In this section, we analyze the performance of our CASCC and fast ML algorithm by simulations, compared with conventional schemes for MIMO-VLC systems.

Let us consider an indoor 2×2 MIMO-VLC scenario as the simulation environment. In (2), let $A_r = 1\text{cm}^2$, $\Phi_{\frac{1}{2}} = 60°$, $\Psi_c = 60°$. The average transmission electrical power is identical in each schemes with SNR defined as $\frac{P_T}{2\sigma^2}$. Here, we use *Matlab* for simulations. LED1 and PD1 are fixed in (0, 0, 0) and (0, 0, 3m), respectively, while LED2 and PD2 randomly move. Here, we take two channels for examples, shown in the following Table 2.

TABLE 2. Two channel scenarios under different locations.

	LED2	PD2	*cond*
$\mathbf{H}_1$	(0, 0.42m, 0)	(0, 2.7965m, 1.5913m)	3.4726
$\mathbf{H}_2$	(0, 1.7818m, 0)	(0, 3.059m, 2.6562m)	1.5042

Following Algorithm 1, we get

$$\mathcal{S}_{B1} = \begin{bmatrix} 0 & 1.3335 & 1.3335 & 0 \\ 0 & 0.0330 & 0.4866 & 0.4536 \end{bmatrix}, \tag{20}$$

$$\mathcal{S}_{B2} = \begin{bmatrix} 0 & 1.1775 & 1.1775 & 0 \\ 0 & 0 & 0.7833 & 0.7833 \end{bmatrix}, \tag{21}$$

with the same $P_T = 4$ for $\mathbf{H}_2$ and $\mathbf{H}_1$, respectively. Then, following Algorithm 2, we can extend the basic constellations $\mathcal{S}_{B1}$, $\mathcal{S}_{B2}$ to the high-order constellations.

1) Constellation Analysis. Fig. 6(a) shows the constellation comparisons amongst CASCC, SM, RC and CC under $\mathbf{H}_1$ with $L = 2^4$, Fig. 6(b) depicts that under $\mathbf{H}_1$ with $L = 2^5$, and Fig. 6(b) plots the similar comparisons under $\mathbf{H}_2$ with $L = 2^5$. Table 3 lists comparisons of $d_{\mathcal{R}m}$ among different schemes under $\mathbf{H}_1$, $\mathbf{H}_2$ with the same $P_T = 4$. For 2×2 MIMO-VLC systems, our CASCC is adapted to different channels, while SM, RC and CC are uniform. The $d_{\mathcal{R}m}$ of CASCC under $\mathbf{H}_1$ and $\mathbf{H}_2$ is 1.4082 and 1.1775, respectively, which is larger than the other schemes. The increased ED makes CASCC outperform SM, RC and CC. Note that as $d_{\mathcal{R}m}$ changes with the total power P_T and constellation size L, the data for parameters in Table 3 are different from the cases in Fig. 6.

2) Complexity and Performance Analysis of Detection. Here, we analyze the complexity and performance analysis of our fast ML detection algorithm. From (17) and (18), we list the computational complexity between conventional ML detection in (14) and our fast Algorithm 3, under different spectral efficiency in Table II. Observed from the

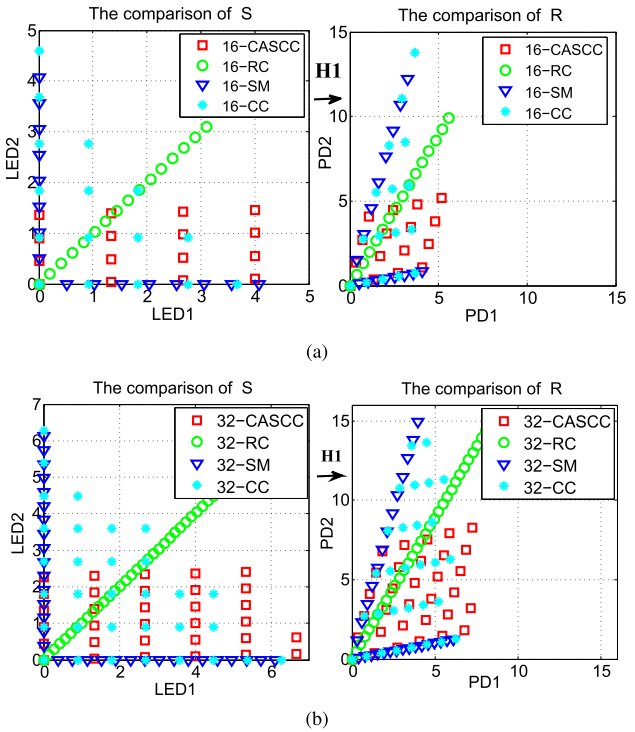

FIGURE 6. Constellation structure comparisons among four schemes under different channels and different constellation sizes. (a) Under $\mathbf{H}_1$ with $L = 2^4$. (b) Under $\mathbf{H}_1$ with $L = 2^5$. (c) Constellation structure comparisons among four schemes under different channels. (d) Under $\mathbf{H}_2$ with $L = 2^5$.

TABLE 3. Comparisons of $d_{\mathcal{R}m}$ for $\mathbf{H}_1$, $\mathbf{H}_2$ with same P_T.

$d_{\mathcal{R}m}$	$cond$	CASCC	SM	RC	CC
$\mathbf{H}_1$	3.4726	1.4082	1.3877	0.6450	0.8327
$\mathbf{H}_2$	1.5042	1.1775	0.6892	0.6325	0.8165

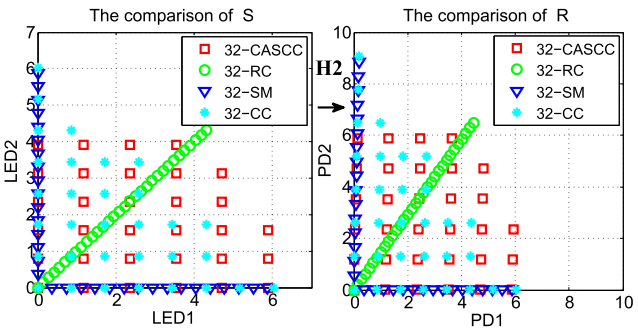

(a) Under $\mathbf{H}_2$ with $L = 2^5$

FIGURE 7. Performance comparisons of conventional detection in (14) and fast detection Algorithm 3 under different scenarios.

results, the low-complexity of our fast ML algorithm is mainly from the deduced search region. Moreover, the more spectral efficiency, the more evident advantage of our Algorithm 3. On another way, Fig. 7 shows the error performance comparisons of conventional ML detection with fast

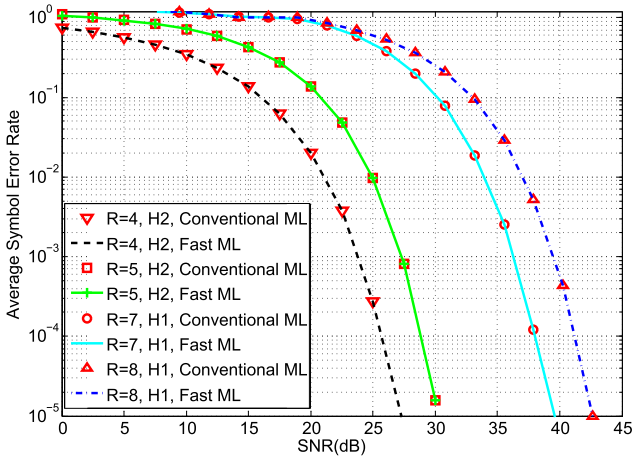

FIGURE 8. Performance comparisons of CASCC, RC, CC and SM, under $\mathbf{H}_1$, at R = 4, 5bit/s/Hz.

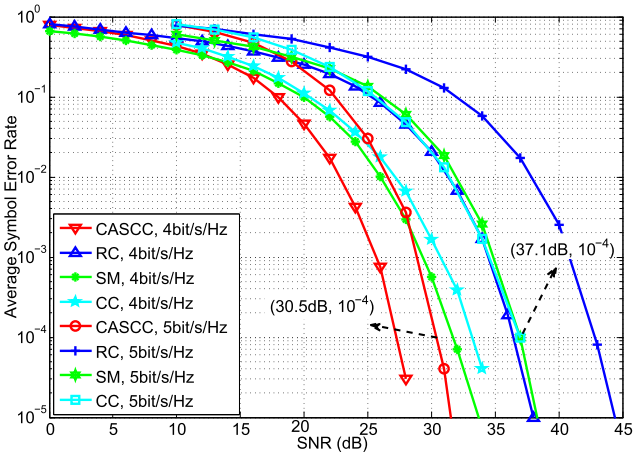

FIGURE 9. Performance comparisons of CASCC, RC, CC and SM, under $\mathbf{H}_1$, at R = 8, 9bit/s/Hz.

Algorithm 3, under different channel and different spectral efficiency. We can observe that our fast ML algorithm efficiently reduces the search region of 2-norm without any error performance loss. Of particularly note is that with rising of B, the complexity of our fast ML algorithm only increases a little.

3) BER Performance Analysis of CASCC. Finally, using our fast ML algorithm, we make the error performance comparisons of our CASCC, with conventional MIMO-VLC schemes, such as CC [15], RC and SM. As shown in Figs. 8 and 9, CASCC achieves 3.6dB, 6.1dB, 13.2dB, 16.3dB gains over SM at a targeted SER of 10^{-5} under $\mathbf{H}_1$ at 4, 5, 8, 9bit/s/Hz, respectively. The higher spectral efficiency, the more gains CASCC achieves over SM at the given channel, which is similar to the RC case. Additionally, CASCC obtains 7.1dB, 7.9dB, 7.6dB, 7.8dB gains over CC at a targeted SER of 10^{-4} under $\mathbf{H}_1$ at 4, 5, 8, 9bit/s/Hz, respectively. There is no obvious change of gains with the increase of B, different from SM, RC. In another way, as

TABLE 4. Complexity comparisons for detection algorithms under different scenarios.

Scenarios	$\mathbf{H}_2$, $B = 4$	$\mathbf{H}_2$, $B = 5$	$\mathbf{H}_1$, $B = 5$	$\mathbf{H}_1$, $B = 7$	$\mathbf{H}_1$, $B = 8$
Conventional ML Detection in (13)	$N_e = 16$ $N_a = 48$ $N_m = 34$	$N_e = 32$ $N_a = 96$ $N_m = 66$	$N_e = 32$ $N_a = 96$ $N_m = 66$	$N_e = 128$ $N_a = 384$ $N_m = 258$	$N_e = 256$ $N_a = 768$ $N_m = 514$
Fast ML Detection in Algorithm 3	$N_e = 6.25$ $N_a = 18.75$ $N_m = 14.5$	$N_e = 7$ $N_a = 21$ $N_m = 16$	$N_e = 6.94$ $N_a = 20.82$ $N_m = 15.88$	$N_e = 7.97$ $N_a = 23.91$ $N_m = 7.94$	$N_e = 8.27$ $N_a = 24.81$ $N_m = 51.62$

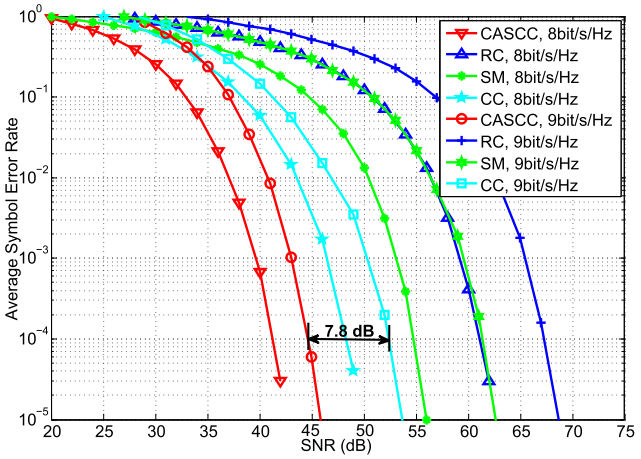

FIGURE 10. Performance comparisons of CASCC, RC, CC and SM, under $\mathbf{H}_2$, at R = 8, 9bit/s/Hz.

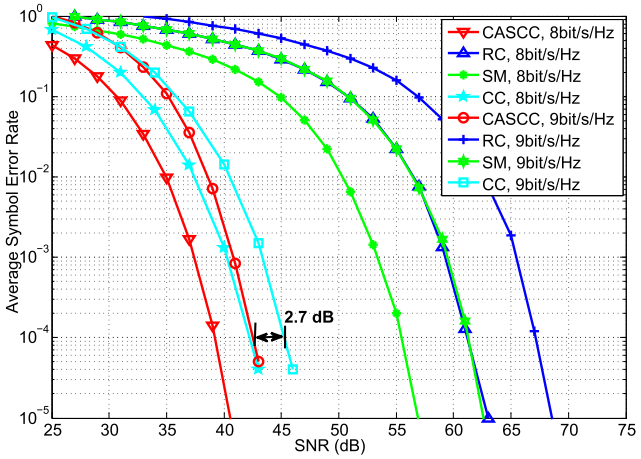

FIGURE 11. Performance comparisons of CASCC, RC, CC and SM, under $\mathbf{H}_2$, at R = 8, 9bit/s/Hz.

shown in Figs. 9 and 11, under $\mathbf{H}_1$ and $\mathbf{H}_2$, CASCC achieves 13.8dB, 16.1dB gains over SM at B = 8bit/s/Hz and a targeted SER of 10^{-5}, whereas CASCC obtains 7.8dB and 2.7dB gains over CC at B = 9bit/s/Hz and a targeted SER of 10^{-4}. Moreover, with the increase of the channel correlation, the superiority of CASCC over SM decreases but remains evident, and the superiority of CASCC over CC becomes larger instead. Note that SM performs even better than CC under $\mathbf{H}_1$ at B = 4bit/s/Hz. In addition, the advantages of CASCC under different channels show that our constellation has a wider application range compared with conventional schemes.

VI. CONCLUSION

In this paper, we have established a general design criterion of CASCC for MIMO-VLC systems. Under the criterion, we particularly designed a regular constellation for 2×2 MIMO-VLC systems in terms of the basic 4-point constellation and the high-order constellation. Correspondingly, we proposed a fast ML detection algorithm without any SER performance loss. In view of the resource utilization, CASCC exploits the spatial resources by building relations amongst LEDs. Furthermore, our objective function is based on the receiver, and thus the proposed constellation design can be utilized to different channels. Simulation results have indicated that our proposed CASCC obtains better error performance and wider applicable range over conventional MIMO-VLC schemes. As to the future research, it is possible to explore the CASCC for larger-size MIMO-VLC systems.

APPENDIX

For conciseness, we list some key notations before all the proofs. The quadrilaterals for $\mathcal{S}_B$, $\mathcal{R}_B$ are denoted as Q_x, Q_y. The diamond Q_y ($\in \mathcal{N}_1$) can be expressed by two parameters of the side length l_f and the angle α_f between two adjacent sides. Let $\Delta\mathbf{R}_{2\times4} \triangleq \mathbf{H}\Delta\mathbf{S}_{2\times4}$, where $\Delta\mathbf{R}_{2\times4} = [\Delta\mathbf{r}_a, \Delta\mathbf{r}_b, \Delta\mathbf{r}_c, \Delta\mathbf{r}_d] = [\mathbf{r}_2 - \mathbf{r}_1, \mathbf{r}_3 - \mathbf{r}_2, \mathbf{r}_4 - \mathbf{r}_3, \mathbf{r}_1 - \mathbf{r}_4]$, $\Delta\mathbf{S}_{2\times4} = [\Delta\mathbf{s}_a, \Delta\mathbf{s}_b, \Delta\mathbf{s}_c, \Delta\mathbf{s}_d] = [\mathbf{s}_2 - \mathbf{s}_1, \mathbf{s}_3 - \mathbf{s}_2, \mathbf{s}_4 - \mathbf{s}_3, \mathbf{s}_1 - \mathbf{s}_4]$. Subscripts $\{1, 2, 3, 4\}$ above are $\mathcal{S}_B$ and $\mathcal{R}_B$, while $\{a, b, c, d\}$ are for $\Delta\mathbf{S}$ and $\Delta\mathbf{R}$.

A. PROOF OF LEMMA 1

Owing to that Q_y in $\mathcal{N}_1$ is a diamond and $\mathcal{R} = \mathbf{H}\mathcal{S}$ above, it is easy to know that Q_x is a parallelogram. The ED of $\mathbf{r}_i$ and $\mathbf{r}_j$ is

$$\begin{aligned}&\|\mathbf{r}_i - \mathbf{r}_j\|^2 \\ &= \left(h_{11}^2 + h_{12}^2\right)(s_{i1} - s_{j1})^2 + (h_{21}^2 + h_{22}^2)(s_{i2} - s_{j2})^2 \\ &\quad + 2(h_{11}h_{21} + h_{12}h_{22})(s_{i1} - s_{j1})(s_{i2} - s_{j2}). \end{aligned} \tag{22}$$

So, $\mathcal{N}_1$ can be partitioned, i.e., $\mathcal{N}_1 = \Omega_1 \cup ... \cup \Omega_k ...$, and all elements from a subset have the equal $|\Delta s_{i1}|, |\Delta s_{i2}|, i \in \{a, b, c, d\}$. Taking Ω_k as example, the performance of $\Delta s_{i1} \cdot \Delta s_{i2} \geq 0$ with ML detector is superior to the other cases at given $\mathbf{H}$, which can be suitable for all the subsets. Therefore, the searching region of the optimal solution to Model 1 can

be reduced to the constellation set of nonnegative slopes of side lengths.

B. PROOF OF LEMMA 2

Q_x in our proposed structure is a parallelogram. The case of $\mathcal{S}$ without the origin is notated as $G_1(\mathbf{m}_1, \mathbf{m}_2, \mathbf{m}_3)$, where the vectors of $\mathbf{m}_1, \mathbf{m}_2$ denote the two adjacent side and the vector $\mathbf{m}_3$ depicts the middle diagonal of $\mathbf{m}_1$ and $\mathbf{m}_2$. Similarly, the case of $\mathcal{S}$ including the origin is denoted as $G_2(\mathbf{n}_1, \mathbf{n}_2, \mathbf{n}_3)$. Let us assume the local optimal constellation for G_1 as $\mathcal{S}_{G1} = [\mathbf{m}_{1\_opt}, \mathbf{m}_{2\_opt}, \mathbf{m}_{3\_opt}, \mathbf{m}_{4\_opt}]$.

Based on the geometrical principles, we have $\|\mathbf{m}_{1\_opt}\|^2 + \|\mathbf{m}_{2\_opt}\|^2 + \|\mathbf{m}_{3\_opt}\|^2 < P_T$ for G_1 and $\|\mathbf{n}_1\|^2 + \|\mathbf{n}_2\|^2 + \|\mathbf{n}_3\|^2 = P_T$ for any values of parameters $\mathbf{n}_{1\_opt}$, $\mathbf{n}_{2\_opt}$, $\mathbf{n}_{3\_opt}$ in G_2. Obviously, there always exist σ_1, σ_2 $\sigma_3 \geq 0$ that meet $\sum_{i=1}^{3} \|\mathbf{m}_{i\_opt} + \sigma_i\|^2 = P_T$. That is to say, a case of parameter values

$$\mathbf{n}_1 = \mathbf{m}_{1\_opt} + \sigma_1, \mathbf{n}_2 = \mathbf{m}_{2\_opt} + \sigma_2, \mathbf{n}_3 = \mathbf{m}_{3\_opt} + \sigma_3, \tag{23}$$

exists for G_2. Apparently, such a case achieves better BER performance than G_1. Therefore, the origin must be in the optimal constellation $\mathcal{S}_{opt}$, i.e., $[0, 0]^T \in \mathcal{S}_{opt}$.

C. PROOF OF LEMMAS 3 AND 4

Using Perron-Frobenius Theorem [20], $\mathbf{H}^T\mathbf{H} = \mathbf{V}\Lambda\mathbf{V}^T$. Let $\Delta\mathbf{R}_{2\times4} \triangleq \mathbf{H}\Delta\mathbf{S}_{2\times4}$, where $\Delta\mathbf{R}_{2\times4} = [\Delta\mathbf{r}_a, \Delta\mathbf{r}_b, \Delta\mathbf{r}_c, \Delta\mathbf{r}_d] = [\mathbf{r}_2 - \mathbf{r}_1, \mathbf{r}_3 - \mathbf{r}_2, \mathbf{r}_4 - \mathbf{r}_3, \mathbf{r}_1 - \mathbf{r}_4]$, $\Delta\mathbf{S}_{2\times4} = [\Delta\mathbf{s}_a, \Delta\mathbf{s}_b, \Delta\mathbf{s}_c, \Delta\mathbf{s}_d] = [\mathbf{s}_2 - \mathbf{s}_1, \mathbf{s}_3 - \mathbf{s}_2, \mathbf{s}_4 - \mathbf{s}_3, \mathbf{s}_1 - \mathbf{s}_4]$. For simplicity, let $\mathbf{b} = [b_1, b_2]^T \triangleq \Delta\mathbf{s}_a$, $\mathbf{a} = [a_1, a_2]^T \triangleq \Delta\mathbf{s}_d$, $\alpha_1 \triangleq |\beta_d|$, $\alpha_2 \triangleq |\beta_a|$, then $dia = \alpha_1 - \alpha_2$.

Then, $\mathbf{D}_{4\times4} \triangleq \Delta\mathbf{R}_{2\times4}^T\Delta\mathbf{R}_{2\times4} = \Delta\mathbf{S}_{2\times4}^T\mathbf{H}^T\mathbf{H}\Delta\mathbf{S}_{2\times4}$. Let

$$\mathbf{G} \triangleq [\mathbf{g}_a, \mathbf{g}_b, \mathbf{g}_c, \mathbf{g}_d] = \mathbf{V}^T\Delta\mathbf{S}, \tag{24}$$

where $\mathbf{g}_i = [g_{i1}, g_{i2}]^T$ for $i \in \{a, b, c, d\}$. Then $\mathbf{D} = \mathbf{G}^T\Lambda\mathbf{G}$. According to our proposed structure, the diagonal elements of $\mathbf{D}_{4\times4}$, denoted as D_{ii}, $i \in \{a, b, c, d\}$ are equal. So, with $\mathbf{D} = \mathbf{G}^T\Lambda\mathbf{G}$, we get

$$l_f^2 = D_{ii} = (g_{i1}\lambda_1)^2 + (g_{i2}\lambda_2)^2, \quad i \in \{a, b, c, d\}. \tag{25}$$

If we use the polar coordinate, Let

$$g_{i1} \triangleq \frac{l_f}{\lambda_1}\cos\beta_i, \quad g_{i2} \triangleq \frac{l_f}{\lambda_2}\sin\beta_i, \tag{26}$$

where $\beta_i \in [0, 2\pi]$. Due to the linearity of VLC channel, Q_x in our proposed structure is a parallelogram, i.e., $\|\Delta\mathbf{s}_a\|_2 = \|\Delta\mathbf{s}_c\|_2$, $\|\Delta\mathbf{s}_b\|_2 = \|\Delta\mathbf{s}_d\|_2$.

1) PROOF OF LEMMA 3

For case I, we have

$$\Delta\mathbf{s}_i = \mathbf{V}\mathbf{g}_i = \begin{bmatrix} \frac{l_f}{\lambda_1}\cos\varphi\cos\beta_i - \frac{l_f}{\lambda_2}\sin\varphi\sin\beta_i \\ \frac{l_f}{\lambda_1}\sin\varphi\cos\beta_i + \frac{l_f}{\lambda_2}\cos\varphi\sin\beta_i \end{bmatrix}, \tag{27}$$

for $i \in \{a, b, c, d\}$. Based on Lemmas 1 and 2, the nonnegative constraint of $\mathcal{S}_E$ can be equivalently transformed as

$$\Delta\mathbf{s}_a, \Delta\mathbf{s}_b \succeq 0 \quad \text{and } \Delta\mathbf{s}_c, \quad \Delta\mathbf{s}_d \preceq 0. \tag{28}$$

Further, it can be rewritten as the constraints to β_a, β_d in Lemma 3 for Case I. As for α_f, when $\alpha_f \neq 0$ and $\alpha_2 = 0$, then $\tan\alpha_f = \tan\alpha_1 = \frac{\Delta r_{4y}}{\Delta r_{4x}}$. When $\alpha_f \neq 0$ and $\alpha_1 = \frac{\pi}{2}$, then $\alpha_f = \frac{\pi}{2} - \arctan\frac{\Delta r_{1y}}{\Delta r_{1x}}$. When $\alpha_f \neq 0, \alpha_1 \neq \frac{\pi}{2}$ and $\alpha_2 \neq 0$, then let $[b_1, b_2]^T \triangleq \Delta\mathbf{s}_a$, $[a_1, a_2]^T \triangleq \Delta\mathbf{s}_d$ for simplicity. From $\Delta\mathbf{R} = \mathbf{H}\Delta\mathbf{S}$, we have $\tan\alpha_1 = \frac{h_{12}a_1 + h_{22}a_2}{h_{11}a_1 + h_{21}a_2}$, $\tan\alpha_2 = \frac{h_{12}b_1 + h_{22}b_2}{h_{11}b_1 + h_{21}b_2}$. Using triangle formulas, we get $\tan\alpha_f = \frac{(h_{12}h_{21} - h_{22}h_{11})(a_1b_2 - a_2b_1)}{a_1b_1(h_{12}^2 + h_{11}^2) + (a_2b_1 + a_1b_2)(h_{12}h_{22} + h_{21}h_{11}) + a_2b_2(h_{22}^2 + h_{21}^2)}$. Based on $\mathbf{H}^T\mathbf{H} = \mathbf{V}\Lambda\mathbf{V}^T$, we get

$$\begin{aligned} h_{11}^2 + h_{12}^2 &= \lambda_1^2\cos^2\varphi + \lambda_2^2\sin^2\varphi, \\ h_{21}^2 + h_{22}^2 &= \lambda_1^2\sin^2\varphi + \lambda_2^2\cos^2\varphi, \\ h_{21}h_{11} + h_{12}h_{22} &= \lambda_1^2\cos\varphi\sin\varphi - \lambda_2^2\sin\varphi\cos\varphi, \\ |h_{12}h_{21} - h_{11}h_{22}| &= \lambda_1\lambda_2. \end{aligned} \tag{29}$$

Substituting (27) and (29) into $\tan\alpha_f$, we get the results in Lemma 3 for Case I. For Case II, we have

$$\Delta\mathbf{s}_i = \mathbf{V}\mathbf{g}_i = \begin{bmatrix} \frac{l_f}{\lambda_1}\cos\beta_i \\ \frac{l_f}{\lambda_2}\sin\beta_i \end{bmatrix}. \tag{30}$$

For Case III, we attain

$$\Delta\mathbf{s}_i = \mathbf{V}\mathbf{g}_i = \begin{bmatrix} -\frac{l_f}{\lambda_2}\sin\beta_i \\ \frac{l_f}{\lambda_1}\cos\beta_i \end{bmatrix}. \tag{31}$$

for $i \in \{a, b, c, d\}$. Owing to that the derivations for Case II and Case III are same as that Case I, it is omitted here. This completes the proof of Lemma 3.

2) PROOF OF LEMMA 4

For Case I, with the relation of $\mathbf{S}$ and $\Delta\mathbf{S}$, we have

$$\begin{aligned} P_T &= \|\mathbf{s}_1\|_2^2 + \|\mathbf{s}_2\|_2^2 + \|\mathbf{s}_3\|_2^2 + \|\mathbf{s}_4\|_2^2 \\ &= \|\Delta\mathbf{s}_a\|_2^2 + \|\Delta\mathbf{s}_d\|_2^2 + \|\Delta\mathbf{s}_a(1) - \Delta\mathbf{s}_d(1)\|_2^2 \\ &\quad + \|\Delta\mathbf{s}_a(2) - \Delta\mathbf{s}_d(2)\|_2^2. \end{aligned} \tag{32}$$

Combining (32) with (27), we can find the relation of l_f with β_a, β_d as $l_f^2 = \frac{P_T}{2T}$, where $T = \frac{\cos^2\beta_a + \cos^2\beta_d - \cos\beta_a\cos\beta_d}{\lambda_1^2} + \frac{\sin^2\beta_a\sin^2\beta_d - \sin\beta_a\sin\beta_d}{\lambda_2^2}$.

For $\mathcal{M}_1$, $d_{\mathcal{R}m1} = l_f$ and so the relation of $d_{\mathcal{R}m1}$ with β_a, β_d is $T = \frac{P_T}{(2d_{\mathcal{R}m1}^2)}$. For $\mathcal{M}_2$, denote the smaller diagonal as d_w, i.e., $d_{\mathcal{R}m2} = d_w$. Based on $\frac{l_1^2}{2(1-\cos\alpha_f)} = {l_f}^2 = \frac{P_T}{2T}$, the relation of $d_{\mathcal{R}m2}$ with β_a, β_d is $d_{\mathcal{R}m2}^2 = d_w^2 = \frac{(1-\cos\alpha_f)}{T}$. This completes the proof of Lemma 4.

D. PROOF OF LEMMA 5

For $\lambda_1 > \lambda_2 = 0$, with $\mathbf{D} = \mathbf{G}^T \Lambda \mathbf{G}$,

$$l_f^2 = (g_{i1}\lambda_1)^2. \tag{33}$$

From $\mathbf{G} = \mathbf{V}^T \Delta \mathbf{S}$, we have

$$\Delta \mathbf{s}_i = \mathbf{V}\mathbf{g}_i = \begin{bmatrix} \frac{l_f}{\lambda_1}\cos\varphi - g_{i2}\sin\varphi \\ \frac{l_f}{\lambda_1}\sin\varphi + g_{i2}\cos\varphi \end{bmatrix}, \tag{34}$$

for $i \in \{a, b, c, d\}$. According to $\Delta \mathbf{s}_a, \Delta \mathbf{s}_b \succeq 0$ and $\Delta \mathbf{s}_c, \Delta \mathbf{s}_d \preceq 0$, if $\varphi \in (0, \frac{\pi}{2})$, we have

$$\begin{cases} \frac{-l_f \cdot \tan\varphi}{\lambda_1} \le g_{12} \le \frac{l_f \cdot \cot\varphi}{\lambda_1} \\ \frac{l_f \cdot \cot\varphi}{\lambda_1} \le g_{42} \le \frac{-l_f \cdot \tan\varphi}{\lambda_1} \le g_{12}. \end{cases} \tag{35}$$

However, there exists no g_{42} meeting the constraints above, which situation also happens to the cases of $\varphi = 0$ and $\varphi = \frac{\pi}{2}$. Therefore, the case of $\lambda_1 > \lambda_2 = 0$ is not in the region of $\mathcal{N}_1$, as concluded in Lemma 5.

E. PROOF OF THEOREM 1

Theorem 1 is proofed in two steps.

Step 1) Proof that CASCC outperforms SM when $M_1 \neq \varnothing$. Denote a and x as the minimum ED for 2^p-SM and 2^p-PAM. For even p, we have $Aa^2 = P_T$, $A = \frac{2^{p-1}(2^{p-1}+1)(2^p+1)}{6}$, and $Ux^2 = P_T$, $U = \frac{(2^{p/2}-1)(2^{(p/2+1)}+1)2^{p+1}}{6}$ at given P_T. It is easy to get $A > U$ though the mathematical induction and thus $a < x$. With similar method applied to the case of odd p, we could also obtain $a < x$. Additionally, PAM$\in M_1$ when $M_1 \neq \varnothing$. Therefore, it could be known that CASCC outperforms over SM under the given P_T.

Step 2) Proof that $M_1 \neq \varnothing$ is equal to $\frac{|det(\mathbf{H})|}{h_{21}h_{11}+h_{12}h_{22}} \ge \sqrt{3}$. Denote $(\frac{\lambda_2\cot\varphi}{\lambda_1}, -\frac{\lambda_2\tan\varphi}{\lambda_1})$ as Point K_1, and $(-\frac{\lambda_2\tan\varphi}{\lambda_1}, \frac{\lambda_2\cot\varphi}{\lambda_1})$ as Point K_2. Obviously, $M_1 \neq \varnothing$ for Submodel 1 is equal to $\max(\frac{\xi(x-y)}{1+xy}) \ge \sqrt{3}$, which is stated in terms of $\xi = 1$ and $\xi = -1$.

i) When $\xi = 1$. Let $f(x, y) = \frac{x-y}{1+xy}$. In one way, differentiate $f(x, y)$ with respect to x and y. Then we get

$$f_x(x, y) = \frac{1+y^2}{(1+xy)^2} > 0, \quad f_y(x, y) = \frac{-1-x^2}{(1+xy)^2} < 0, \tag{36}$$

which means no extreme value for $f(\cdot)$. In another way, analyze the boundary of region in Lemma 3. Then we find that $f(x, y)$ gets its maximum value at K_1 and its minimum value at K_2, i.e.,

$$\begin{aligned} f_{max} &= f(K_1) = \frac{\lambda_1\lambda_2(\tan\varphi + \cot\varphi)}{(\lambda_1^2 - \lambda_2^2)}, \\ f_{min} &= f(K_2) = -f_{max} \le 0. \end{aligned} \tag{37}$$

Based on (29), we can get $f_{max} = \frac{|det(\mathbf{H})|}{h_{21}h_{11}+h_{12}h_{22}}$.

ii) When $\xi = -1$. Let $g(x, y) = \frac{-x+y}{1+xy}$. It can be observed that $g(x, y) = -f(x, y)$. Then we have $g_{min} = g(K_1)$ and $g_{max} = g(K_2) = \frac{|det(\mathbf{H})|}{h_{21}h_{11}+h_{12}h_{22}}$. Therefore, CASCC outperforms SM when $\frac{|det(\mathbf{H})|}{h_{21}h_{11}+h_{12}h_{22}} \ge \sqrt{3}$. This completes the proof of Theorem 1.

REFERENCES

[1] T. Komine and M. Nakagawa, "Fundamental analysis for visible-light communication system using LED lights," *IEEE Trans. Consum. Electron.*, vol. 50, no. 1, pp. 100–107, Feb. 2004.

[2] A. Jovicic, J. Li, and T. Richardson, "Visible light communication: Opportunities, challenges and the path to market," *IEEE Commun. Mag.*, vol. 51, no. 12, pp. 26–32, Dec. 2013.

[3] S. Rajbhandari *et al.*, "High-speed integrated visible light communication system: Device constraints and design considerations," *IEEE J. Sel. Areas Commun.*, vol. 33, no. 9, pp. 1750–1757, Sep. 2015.

[4] L. Zeng *et al.*, "High data rate multiple input multiple output (MIMO) optical wireless communications using white led lighting," *IEEE J. Sel. Areas Commun.*, vol. 27, no. 9, pp. 1654–1662, Dec. 2009.

[5] A. Burton, H. L. Minh, Z. Ghassemlooy, E. Bentley, and C. Botella, "Experimental demonstration of 50-Mb/s visible light communications using 4 × 4 MIMO," *IEEE Photon. Technol. Lett.*, vol. 26, no. 9, pp. 945–948, May 1, 2014.

[6] I. Din and H. Kim, "Energy-efficient brightness control and data transmission for visible light communication," *IEEE Photon. Technol. Lett.*, vol. 26, no. 8, pp. 781–784, Apr. 15, 2014.

[7] S. G. Wilson, M. Brandt-Pearce, Q. Cao, and M. Baedke, "Optical repetition MIMO transmission with multipulse PPM," *IEEE J. Sel. Areas Commun.*, vol. 23, no. 9, pp. 1901–1910, Sep. 2005.

[8] R. Mesleh, R. Mehmood, H. Elgala, and H. Haas, "Indoor MIMO optical wireless communication using spatial modulation," in *Proc. IEEE Int. Conf. Commun.*, May 2010, pp. 1–5.

[9] M. D. Renzo and H. Haas, "Spatial modulation for generalized MIMO: Challenges, opportunities, and implementation," in *Proc. IEEE*, vol. 102, no. 1, pp. 56–103, Jan. 2014.

[10] R. Mesleh, H. Elgala, and H. Haas, "Optical spatial modulation," *IEEE J. Opt. Commun. Netw.*, vol. 3, no. 3, pp. 234–244, Mar. 2011.

[11] T. Fath and H. Haas, "Performance comparison of MIMO techniques for optical wireless communications in indoor environments," *IEEE Trans. Commun.*, vol. 61, no. 2, pp. 733–742, Feb. 2013.

[12] A. Nuwanpriya, S.-W. Ho, and C. S. Chen, "Indoor MIMO visible light communications: Novel angle diversity receivers for mobile users," *IEEE J. Sel. Areas Commun.*, vol. 33, no. 9, pp. 1780–1792, Sep. 2015.

[13] H. Song and M. Brandt-Pearce, "A 2-D discrete-time model of physical impairments in wavelength-division multiplexing systems," *J. Lightw. Technol.*, vol. 30, no. 5, pp. 713–726, Mar. 1, 2012.

[14] H. Song and M. Brandt-Pearce, "Range of influence and impact of physical impairments in long-haul DWDM systems," *J. Lightw. Technol.*, vol. 31, no. 6, pp. 846–854, Mar. 15, 2013.

[15] Y.-J. Zhu, W.-F. Liang, J.-K. Zhang, and Y.-Y. Zhang, "Space-collaborative constellation designs for MIMO indoor visible light communications," *IEEE Photon. Technol. Lett.*, vol. 27, no. 15, pp. 1667–1670, Aug. 2015.

[16] H.-B. Cai, J. Zhang, Y.-J. Zhu, J.-K. Zhang, and X. Yang, "Optimal constellation design for indoor 2×2 MIMO visible light communications," *IEEE Commun. Lett.*, vol. 20, no. 2, pp. 264–267, Feb. 2016.

[17] M. Beko and R. Dinis, "Systematic method for designing constellations for intensity-modulated optical systems," *IEEE J. Opt. Commun. Netw.*, vol. 6, no. 5, pp. 449–458, May 2014.

[18] J. Karout, E. Agrell, and K. Szczerba, "Optimizing constellations for single-subcarrier intensity-modulated optical systems," *IEEE Trans. Inf. Theory*, vol. 58, no. 7, pp. 4645–4659, Jul. 2015.

[19] A. Chaaban, Z. Rezki, and M.-S. Alouini, "Fundamental limits of parallel optical wireless channels: Capacity results and outage formulation," *IEEE Trans. Commun.*, vol. 65, no. 1, pp. 296–311, Jan. 2017.

[20] C. D. Meyer, *Matrix Analysis and Applied Linear Algebra Book and Solutions Manual*. Philadelphia, PA, USA: Society for Industrial and Applied Mathematics, 2000.

[21] K. Xu, H. Yu, and Y. J. Zhu, "Channel-adapted space-collaborative constellation design for MIMO visible light communication," in *Proc. IEEE GLOBECOM*, Washington, DC, USA, Dec. 2016, pp. 1–7.

KE XU received the B.S. degree from the National Digital Switching System Engineering & Technological Research Center (NDSC), Zhengzhou, China, in 2014. She is currently pursuing the M.S. degree in communications and information system with NDSC. Her main research interests are in the areas of wireless communication theory, visible light communications, and signal processing.

HONG-YI YU received the M.Sc. degree from the Department of Communication Engineering, Zhengzhou Information Science and Technology Institute, China, in 1987, and the Ph.D. degree from Xidian University in 1999. He is currently with the National Digital Switching System Engineering & Technological Research Center, Zhengzhou, China. His main research interests are in the areas of wireless communication theory, visible light communications, and signal processing.

YI-JUN ZHU (M'14) received the B.Eng., M.Sc., and Ph.D. degrees from the Department of Communication Engineering, Zhengzhou Information Science and Technology Institute, China, in 1999, 2002, and 2010, respectively. During 2011, he was a Visitor with the Department of Electrical and Computer Engineering, McMaster University. He is currently with the National Digital Switching System Engineering & Technological Research Center, Zhengzhou, China. His main research interests are in the areas of wireless communication theory, visible light communications, and signal processing.

HENG-BIN CAI received the B.S. and M.S. degrees from the National Digital Switching System Engineering & Technological Research Center (NDSC), Zhengzhou, China, in 2014. He is currently involving in communications and information system with NDSC. His main research interests are in the areas of wireless communication theory, visible light communications, and signal processing.